LARGE EDDY SIMULATION OF REACTIVE TWO-PHASE FLOW IN AN AERONAUTICAL MULTIPOINT BURNER

G. Hannebique, P. Sierra, E. Riber, B. Cuenot

hannebiq@cerfacs.fr

CERFACS, 42 Avenue Gaspard Coriolis, 31057 Toulouse Cédex 01, France

Abstract

Due to compressibility criteria, fuel used in aeronautical combustors is liquid. Numerical simulation therefore requires the modeling of two-phase flames, involving key phenomena such as injection, atomization, coalescence, polydispersion, drag, evaporation and turbulent combustion. In the present work, particular modeling efforts have been made on spray injection and evaporation, and their coupling to turbulent combustion models in the Large Eddy Simulation (LES) approach. The model developed for fuel injection is validated against measurements in a non-evaporating spray in a quiescent atmosphere, while the evaporation model accuracy is discussed from results obtained in the case of evaporating isolated droplets. These models are finally used in reacting LES of a multipoint burner in take-off conditions, showing the complex two-phase flame structure.

Introduction

Large Eddy Simulation (LES) is a powerful tool to simulate industrial-scale burners and to understand complex unsteady phenomena such as combustion instabilities, ignition or quenching, giving access to the large scales structures and reducing the importance of modeling. Since many combustion systems burn liquid fuel, extending LES to spray flames is crucial but still challenging, mainly because the physical submodels required to describe the atomization of a liquid fuel jet, the dispersion of fuel droplets, their interaction with walls, evaporation and combustion are essentially subgrid phenomena. Direct simulation using interface tracking methods [1, 2, 3] is promising but still unaffordable in complex geometries. Therefore, Euler-Euler and Euler-Lagrange approaches are widely used to perform LES in complex geometries [4, 5, 6].

In this work, the Euler-Euler approach detailed in [5] is used in a multipoint burner where liquid kerosene is injected by both a pilot and a series of liquid jets distributed around it, and the air is swirled through a complex premixing swirler. Previous comparisons with Euler-Lagrange simulations and experiments in complex geometries [4, 7] showed that the Euler-Euler approach provides accurate results for non-reacting two phase flows. The objective of this work is to perform a reacting two-phase LES in realistic take-off conditions to investigate the effects of complex liquid kerosene injection on the combustion process. First, models used for injection and evaporation which are key phenomena are tested in academic configurations and compared with measurements. Then, results of the two-phase cold and reacting LES are analysed, enhancing the impact of the double-injection on the flame. Finally, the structure of the resulting spray flame is analysed in details to provide information for chemistry and combustion modeling in the context of two-phase combustion in complex configurations.

Injection modeling using the FIM-UR approach

In many aeronautical burners, liquid fuel is injected in the burner in the form of a dilute spray, characterized by a droplet size distribution and air-fuel velocity fields. The spray is usually

generated by an air-blast atomizer, and is the result of complex processes, initiated inside the injector itself and involving interaction with the air flow [8]. The liquid jet exiting from the injector is first submitted to strong shear from the air flow leading to primary atomization. In a second phase, secondary atomization occurs through interactions with the air and between droplets. In the same time, drag force and evaporation modify the gas flow and composition in the spray. Simulating primary atomization is a challenging and still open problem [1, 2, 3], which requires the description of liquid/gas interface, and is today out of reach in LES of complex two-phase reacting flows. The FIM-UR model proposed in [4] circumvents the atomization issue for two-phase LES by building from global and geometrical characteristics the profiles of the liquid volume fraction, gas and liquid velocity and droplet size at the close vicinity of the injector. To illustrate the model and assess its accuracy, the simple configuration of [9] has been computed and compared to experimental results.

The configuration is a simple cylindrical chamber with a pressure-swirl Delavan atomizer injecting kerosene with a mass flow rate of $3g.s^{-1}$ in a quiescent atmosphere. Initial gas and liquid temperatures are both $300K$. The spray is assumed monodisperse with a droplet mean diameter of $55\mu m$. The half-spray angle is 30 degrees.

Figures 1a. and b. show the computational domain and a vertical mid-plane cut of the mesh respectively. Two-phase LES was performed using the TTGC scheme [10], the WALE subgrid scale model [11] and the NSCBC method [12] for the gas phase, as well as the TTGC scheme, the Moreau subgrid scale model [13] and Dirichlet boundary conditions for the dispersed phase.

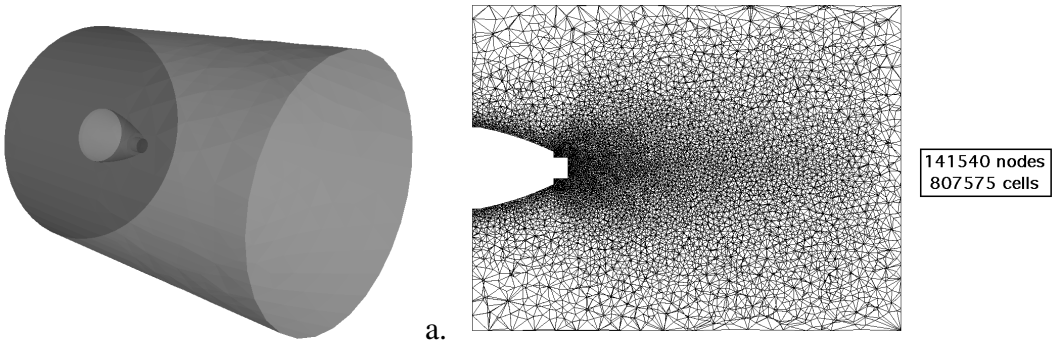

a. b.

Figure 1. (a.) Injection test case geometry. (b.) Fieldview of the mesh.

Figure 2 shows a qualitative comparison of the observed and computed spray topologies. The experimental direct visualization in Fig. 2a. shows a half-spray angle of 30 degrees. These characteristics are well reproduced in the computed spray, as shown in Fig. 2b. The hollow cone structure is also well reproduced. This indicates that the FIM-UR injection model correctly sets the liquid velocity and volume fraction and that the monodisperse assumption is acceptable in this case. To better assess the validity of the model, mean liquid axial velocity profiles obtained from the LES are compared to the measurements in Fig. 3 at various axial distances from the injector nozzle, indicated in Fig. 2b. The overall shape and level are in good agreement with the experimental results. Droplets are slowed by the gas phase, although far from the tip, discrepancies appear due to the coarsening of the mesh far from the nozzle. LES using both Euler-Euler and Euler-Lagrange approaches on a more refined grid are being performed to increase the accuracy and to validate more precisely the Euler-Euler approach in this configuration.

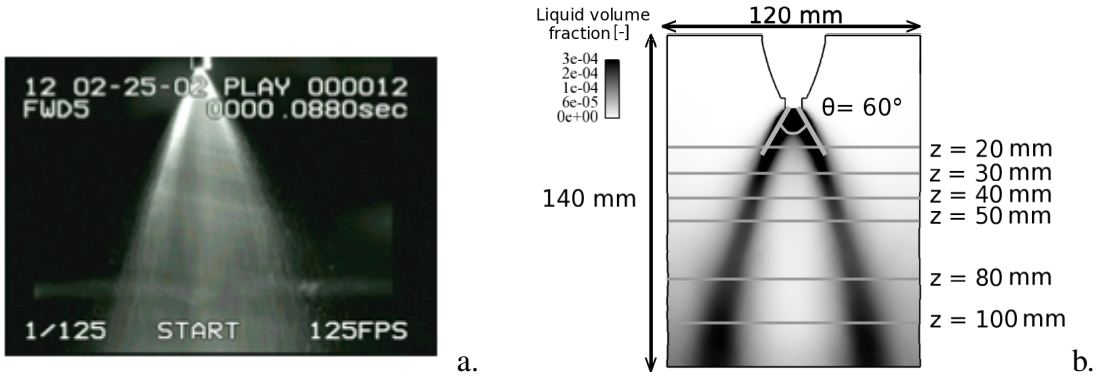

Figure 2. Qualitative comparison of spray topologies: experimental direct visualization (a.) and mean liquid volume fraction field in the mid-plane from simulation (b.).

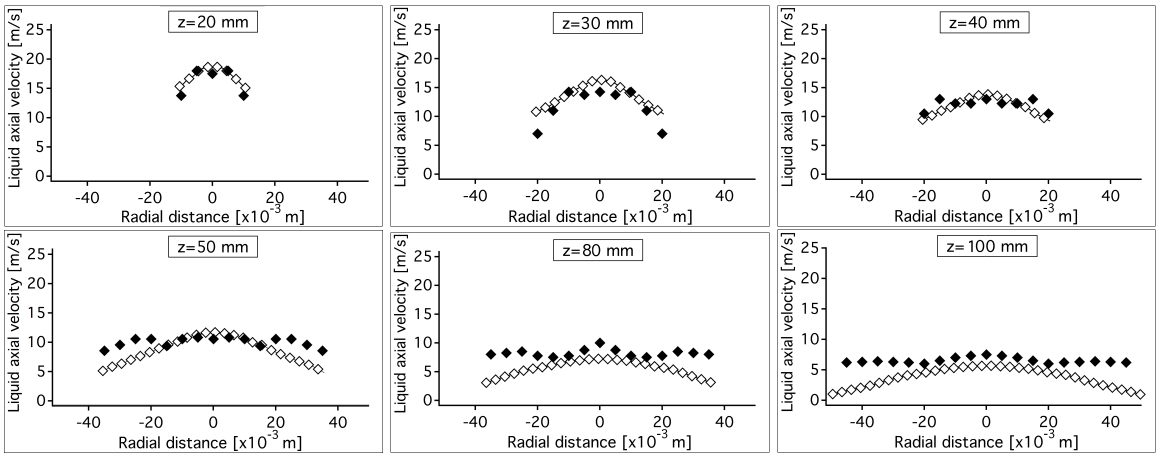

Figure 3. Radial profiles of mean liquid axial velocity at various stations downstream of the injector nozzle. Comparison between experiments(⧫) and simulation (◊).

Evaporation modeling

With two-phase combustion in prospect, the evaporation model is crucial to determine the fuel vapor field. The model used in AVBP (referred hereafter as 'AVBP-standard') assumes infinite conduction in the liquid and spherical symmetry of the droplet. The gas is considered quasi-stationary, so the thermal and mass transfers in the gas phase only depend on the distance to the surface of the droplet [5]. Up to recently, all the experiments measuring the diameter temporal evolution of an evaporating isolated droplet were conducted with the droplet suspended on a support fiber to avoid the experimental difficulties of free-falling droplets [14]. Chauveau *et al.* [15] recently proposed to use a novel cross micro-fiber system in order to reduce the diameter of the fiber and consequently the effect of heat conduction through the fiber, keeping the spherical shape of the droplet. Repeating the experiments from the literature of a n-heptane droplet evaporating in a N_2 quiescent atmosphere, the evaporation time was almost doubled. In parallel simulating the same experiments, Sanjosé [16] showed that the evaporation process is strongly influenced by the modelisation of the mixture thermodynamical properties. Based on this last observation, a new evaporation model is proposed here and compared both to the 'AVBP-standard' model and to experiments [14, 15].

The Abramzon-Sirignano model [17] is used to compute the mass transfer rate Γ and the

heat transfer composed of two contributions, the conductive flux Φ_g and the enthalpy flux Λ_g due to phase exchange:

$$\Gamma = -\pi d_p Sh[\rho D_F] ln(1+B_M) \,, \tag{1}$$

$$\Phi_g = -\pi d_p Nu \lambda (T_{\inf} - T_l) \frac{ln(1+B_T)}{B_T} \,, \tag{2}$$

$$\Lambda_g = \Gamma h_{s,F}(T_l) \,, \tag{3}$$

where d_p is the droplet diameter, Sh and Nu are respectively the Sherwood and the Nusselt numbers following the Ranz-Marshall correlations [18], D_F is the fuel diffusivity, $B_M = (Y_{F,\zeta} - Y_{F,\inf}) / (1 - Y_{F,\zeta})$ is the Spalding mass number, $B_T = (1+B_M)^\beta$ is the thermal Spalding number ($\beta = C_{p,F}/C_p \times Sh \cdot Pr/Nu \cdot Sc$, $C_{p,F}$ stands for the gaseous fuel heat capacity, C_p is the heat capacity of the mixture), and Pr and Sc are the mixture Prandtl and Schmidt numbers. Note that ζ stands for the properties calculated at the droplet surface and $Y_{F,\zeta}$ is calculated using the Clasius-Clapeyron law. Thermodynamic and transport properties are computed using the reference state corresponding to the 1/3 law [19] which assumes that the properties in the gaseous film surrounding the droplet follow a quasi-stationary evolution. The so-called 'AVBP-standard' and 'AVBP-mix' models differ from the thermodynamic and transport properties used.

In the 'AVBP-standard' model, the product $[\rho D_F]$ is considered as constant between the droplet surface and the infinity and yields:

$$[\rho D_F] = \frac{\mu(T_{ref})}{Sc_F} \,, \tag{4}$$

where Sc_F is the fuel Schmidt number considered as constant, T_{ref} is the reference temperature and μ is the mixture viscosity evaluated by a Power law dependence upon temperature. The Prandtl and Schmidt numbers are taken equal to those used for the gas flow simulation.

There are two improvements in the 'AVBP-mix' model. First, the Prandtl and Schmidt numbers of the mixture are deduced from equilibrium calculations using the CANTERA software [20], being more realistic. Second, the mixture viscosity still evaluated at the reference temperature also depends on mixture composition following the Wilke relation [21]:

$$\mu = \sum_i \frac{X_i \mu_i}{\sum_j X_j \Phi_{ij}} \,, \tag{5}$$

$$\Phi_{ij} = \frac{1}{\sqrt{8}} \left(1 + \frac{W_i}{W_j}\right)^{-1/2} \left[1 + \left(\frac{\mu_i}{\mu_j}\right)^{1/2} \left(\frac{W_j}{W_i}\right)^{1/4}\right]^2 \,, \tag{6}$$

where μ_i is the vicosity of species i in the gas mixture, being fitted with a power law on temperature using CANTERA database.

Using Eqs. (5) and (6), the 'AVBP-mix' model should be close to the Chapman-Enskog kinetic therory of gases used in CANTERA for instance. Indeed, the main differences are the species diffusion coefficients which depend on the binary diffusion coefficients, and the thermal conductivity of the mixture which is a combination of the thermal conductivity of each species in the mixture. Modeling evaporation using the kinetic theory in AVBP would be very expensive due to the computation of integral collisions. A solution is to couple CANTERA with AVBP ('AVBP-CANTERA' model) to assess the accuracy of the 'AVBP-mix' evaporation model by comparison with the kinetic theory in academic configurations.

	Fuel	Gas	Pressure [atm]	Gas temperature [K]	Droplet temperature [K]	Droplet diameter [μm]
Case 1	n-heptane	N_2	1	623	300	500
Case 2	kerosene	air	19	728	300	10

Table 1. Initial conditions for the simulation of isolated droplet evaporating in a quiescent atmosphere.

Table 1 details the initial conditions for the two simulations of an isolated droplet evaporating in a quiescent atmosphere. Case 1 corresponds to the academic case of [14] repeated in [15] whereas Case 2 corresponds to the evaporation conditions of a kerosene droplet outing from the pilot injection of the TLC configuration. Figure 4 shows the temporal evolution of the droplet diameter and temperature for Case 1. The transport and thermodynamic properties in the evaporation model considerably affect the evaporation time: using 'AVBP-mix', the evaporation time is doubled compared to 'AVBP-standard', being close to the measurements of Chauveau *et al.* The comparison of 'AVBP-mix' and 'AVBP-CANTERA' results shows that accounting for the mixture composition to evaluate the mixture viscosity using a power law dependence for each species viscosity is sufficient to correctly reproduce the mixture viscosity. The evaporation model also has a non-negligible impact on the liquid temperature, as displayed in Fig. 4b. The same behaviour is observed for the droplet of kerosene in Case 2 (Fig. 5). New experimental results are necessary both to validate the method used in [15] and to characterize evaporation of kerosene.

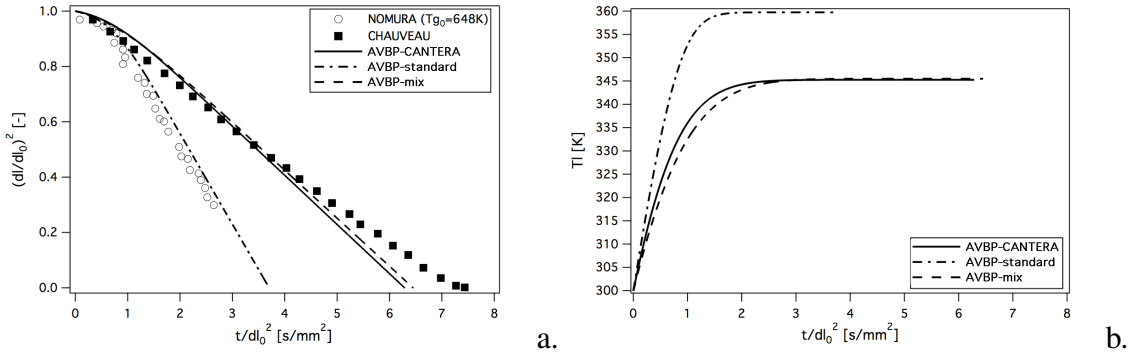

Figure 4. Temporal evolution of squared droplet diameter (a.) and liquid temperature (b.) for Case 1 in Table 1. Comparison between measurements [14, 15] and simulations using 'AVBP-standard', 'AVBP-mix' and 'AVBP-CANTERA' models.

Application to the TLC configuration

The application configuration was set-up in the framework of the TLC (Towards Lean Combustion) European Project and is representative of a multipoint burner, where liquid fuel is injected by both a pilot and a series of liquid jets distributed around it, and the air is swirled through a complex premixing swirler. The computational domain shown in Fig. 6 includes a multipoint injection system and a swirler around it, a plenum for air supply, a chamber and an exit nozzle.

Details of the pilot and the multipoint fuel injectors are provided in Fig. 7a. The pilot fuel atomizer is of the so-called piezo-type, and a series of 24 holes of diameter of $0.5mm$, located on the inner wall of the main stage form the multipoint injector. The fuel distribution among the

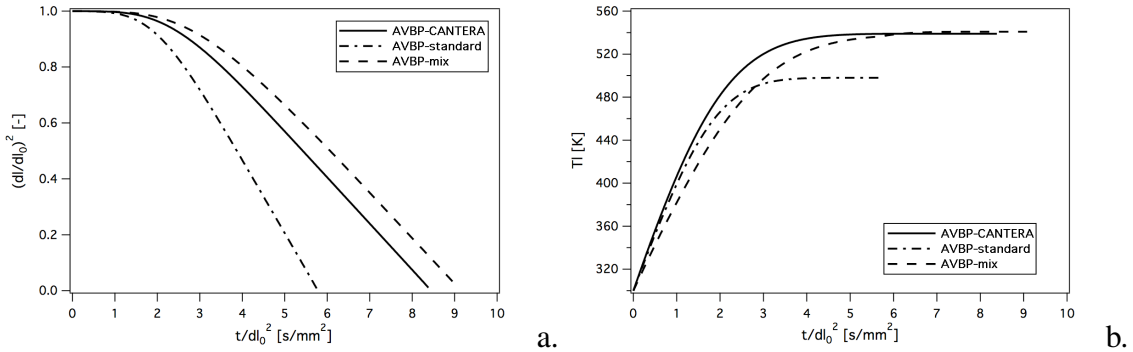

Figure 5. Temporal evolution of squared droplet diameter (a.) and liquid temperature (b.) for Case 2 in Table 1. Comparison between simulations using 'AVBP-standard', 'AVBP-mix' and 'AVBP-CANTERA' models.

Figure 6. Computational domain for the TLC configuration.

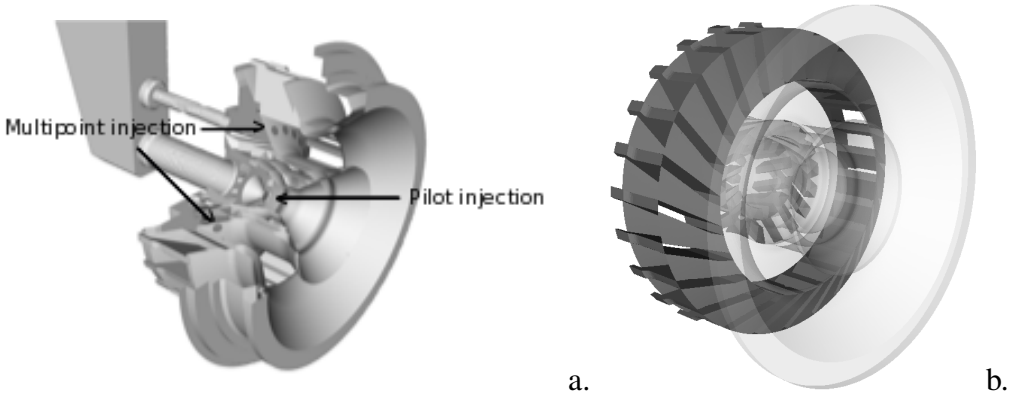

Figure 7. Close view of the two injection systems (a.) and the three swirler stages (b.).

two systems depends on the operation regime. The premixing swirler has three stages as shown in Fig. 7b. All stages are counter-rotating relative to each other, which increases the turbulent mixing in the areas where the different flows meet. Approximately 90% of the total air goes through the main swirler stage. The remaining 10% is split between the inner (3%) and the outer pilot swirlers (7%). Multiperforated walls are used to provide cooling air to the chamber. At the choked exit nozzle, supersonic flow conditions lead to acoustically non-reflecting outflow boundary condition.

The computed operating point corresponds to take-off conditions (full thrust), where both fuel injectors are fed with kerosene at temperature $T_l = 300K$. Droplets with a diameter of

$10\mu m$ and a half spray angle of 30 degrees are injected at the pilot injector nozzle using the FIM-UR model whereas droplets with a diameter of $30\mu m$ are injected perpendiculary to the hole surface of the multipoint injector. 15% of kerosene is injected through the pilot injector. Air is injected at temperature $Tg = 728K$. The fuel/air ratio corresponds to a global equivalence ratio of 0.44. The chamber pressure is $19.5\ bars$.

The simulation was performed with AVBP using the mesh illustrated in Fig. 8. It is strongly refined in the mixing and reactive zones, around the swirlers and the injection systems. The same models and boundary conditions as for the liquid injection simulation were used. Concerning numerics, the Lax-Wendroff scheme [22] and the PSI scheme [23] were used for the gas and the dispersed phase respectively. Moreover, the 2S_KERO_BFER two-step reduced scheme for kerosene-air flames [24] was used. It accounts for a kerosene oxidation reaction and the CO-CO2 equilibrium, and has been fitted against experimental data and detailed mechanisms to reproduce correctly the laminar flame speed and the burnt gas temperature over a wide range of pressure, temperature and equivalence ratio. The Dynamic Thickening flame model [25] was used to model flame-turbulence interactions.

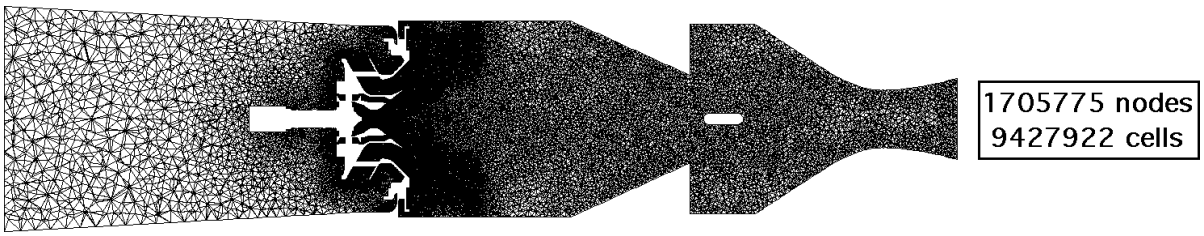

Figure 8. Vertical mid-plane cut of the mesh used for the TLC configuration.

Results - Cold flow

Figure 9a. shows the gas mean axial velocity field in a vertical cut plane of the combustion chamber. Under the effect of swirl, the flow opens largely when entering the chamber and different recirculation zones appear: a central toroidal recirculation zone occupies a large volume of the chamber and enters into the diffuser of the injection system. Corner recirculation zones also develop in the usptream corners of the chamber. Strong shear layers appear in the regions where the flows issued from the different stages meet, as shown by the gas root-mean square (RMS) axial velocity field in Fig 9b. In these zones, the turbulence intensity reaches 25%, leading to strong mixing. Validation of LES in the same geometry but for a smaller chamber pressure ($P = 4.37\ bars$) was proposed in [7] by comparison with experiments.

Results - Reactive case

A global picture of the two-phase flame is given in Fig. 10 with the mean liquid volume fraction field and an isoline of heat release. It clearly shows how the liquid kerosene enters the chamber through both injection lines, follows the opening air flow and evaporates upstream and inside the flame front. A conical flame is obtained, stabilized by both injections and extending around the recirculation zone, in the high shear region. This flame produces hot gases at a temperature close to 2600 K (corresponding to the stoichiometric burnt gas temperature) that fill the central recirculation zone (Fig. 10b.). These gases do not mix immediately with the surrounding cold flow, resulting in a quite inhomogeneous temperature distribution in the first half of the chamber. Mixing is however almost complete in the second half of the chamber, resulting in a significant decrease of the temperature at the chamber exit. Figure 10b. also shows that in the second half of the chamber, *i.e.* in a well mixed region, the computed mean temperature profile is relatively flat, with a mean value ($T_{mean} = 1796K$) almost equal to the burnt gas temperature at the global

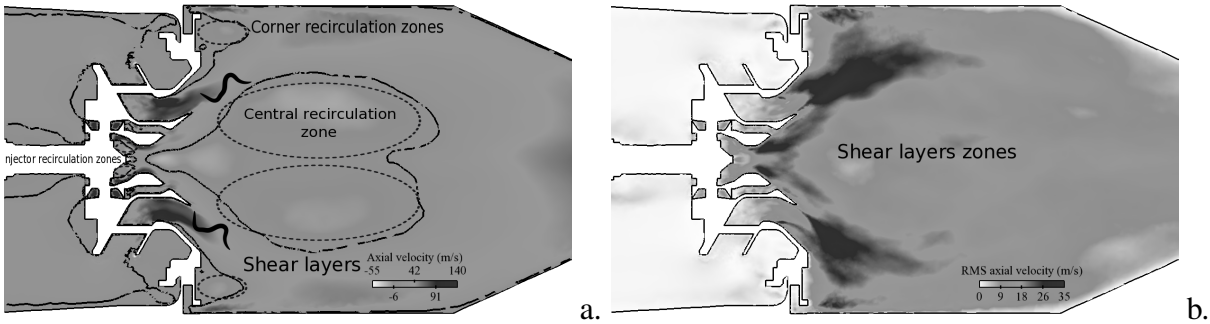

a. b.

Figure 9. Flow topology in the TLC chamber. (a.) Mean gas axial velocity field in the vertical cut plane, with the zero-axial gas velocity isoline (black line). (b.) RMS gas axial velocity field in the vertical cut plane. High shear zones are indicated by high fluctuations.

equivalence ratio of the simulation ($T_{BG} = 1793K$) as expected.

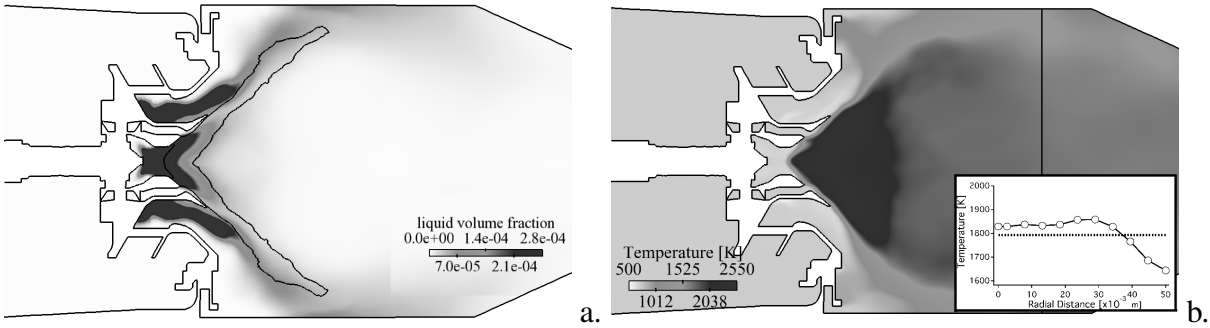

a. b.

Figure 10. (a.) Mean liquid volume fraction field in the vertical mid-plane cut, with mean heat release isoline (black line, value $4.6 \times 10^9 J/m3/s$). (b.) Mean gas temperature in the vertical mid-plane cut with radial profile of mean temperature compared to the burnt gas temperature at global equivalence ratio $\phi = 0.44$.

The local flame structure depends on the spray dispersion and evaporation, resulting in a non-homogeneous field of kerosene vapor which in turn mixes with the ambiant air. Figure 11a. shows an instantaneous field of fuel vapor, together with an isoline of evaporation mass transfer (in grey) and an isoline of heat release (in black). Evaporation mainly occurs in the fresh gases close to the injector exit. In the present operation conditions, saturation is reached rapidly in the evaporating pilot spray and the time needed to evaporate all the liquid is about $1ms$, while the convective time needed to reach the flame is much smaller ($0.225ms$). In addition, most of the droplets issued from the pilot are stopped by the central recirculation zone, where the flame stabilizes, and complete their evaporation there. As a consequence, evaporation also occurs in the flame and in the burnt gases. This is not the case for the droplets injected through the multipoint injector: even if saturation is reached rapidly next to injection, the liquid volume fraction decreases enough to enable evaporation, with a caracteristic evaporation time close to $0.6ms$ which is smaller than the convective time $0.7ms$. This leads to a complex flame structure, as will be seen later.

The liquid injections result then in a partially premixed flame, experiencing variable equivalence ratio. The small droplets issued from the central pilot evaporate enough strongly to create a rich premixed flame in the close vicinity of the injector, producing burnt gases without oxygen. The remaining droplets go through the flame, accumulate and evaporate just behind, leading to a high fuel vapor concentration in this region which mixes with the oxygen-free burnt

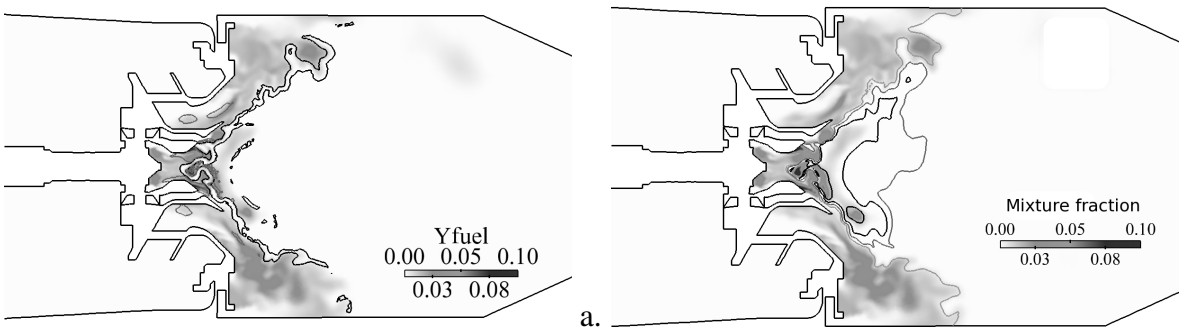

Figure 11. (a.) Instantaneous fuel vapor field in the vertical mid-plane cut, with isolines of heat release (black line) and evaporation mass transfer (grey line), black arrows showing mass tranfert isolines. (b.) Instantaneous mixture fraction field in the vertical mid-plane cut, with isolines of temperature: black $T = 2500K$, dark grey $T = 2000K$, light grey $T = 1500K$.

gases. The liquid injected by the multipoint system being more diluted when reaching the flame, gives smaller equivalence ratio. The resulting field of mixture fraction Z is shown in Fig. 11b. where isolines of temperature are superimposed. Note that Z is based on the C atom as:

$$Z = \frac{Y_C - Y_C^O}{Y_C^F - Y_C^O} \ , \tag{7}$$

where Y_C is the mass fraction of the C atom, and the superscripts O and F refer to the pure oxidizer and pure fuel streams respectively. In the present case, $Y_C^O = 0$ and the mixture fraction reduces to $Z = Y_C/Y_C^F$, varying from 0 in pure air to 1 in pure kerosene. The stoichiometric value is $Z_{st} = 0.0625$. As diluted kerosene sprays are injected in the present configuration, the maximum value of Z obtained in the calculation does not exceed 0.2. The mixture fraction gradually increases from the injectors downstream of the flame, and continues to increase in the burnt gases behind the flame in the tip region of the central recirculation zone, while it stays close to stoichiometry or below in the rest of the chamber, where it finally goes back to the global value. Interestingly, the flame follows the stoichiometric isoline as long as it exists in the fresh reactants. This is the consequence of the variable equivalence ratio through the flame, due to evaporation, and leading to a maximum heat release at stoichiometry. Note also that the downstream parts of the flame front burn at an equivalence ratio close to the lean flammability limit ($\phi = 0.4$).

To understand the flame structure, the Takeno index is calculated to identify the local combustion regimes. Results are given in Fig.12. The index is normalized to be 1 in premixed flames and -1 in diffusion flames, and is conditionned by the reaction zones. A first observation is that this index reveals an additional diffusion flame downstream of the main premixed flame, which was too weak to be visible in the previous pictures. This flame is the result of the burning of the very rich, oxygen-free burnt gas pocket generated by the pilot spray evaporation, with the oxygen coming from the external swirler stage, in a fully non-premixed regime. Otherwise the whole flame is premixed, with variable equivalence ratio and a particular structure revealed by the change of sign of the Takeno index in the burnt side of the flame: this is due to the change of sign of the fuel vapor gradient, which increases again under the effect of spray evaporation. In this zone, although the Takeno index is negative, the combustion regime is still premixed, with a variable equivalence ratio accross the flame.

This particular structure is characterized in Fig. 13 with scatterplots of fuel vapor and temperature versus mixture fraction. In Fig. 13b., the chemical equilibrium solution is plotted with white symbols as a reference. The scatter plots reveal two limits. The first one corresponds

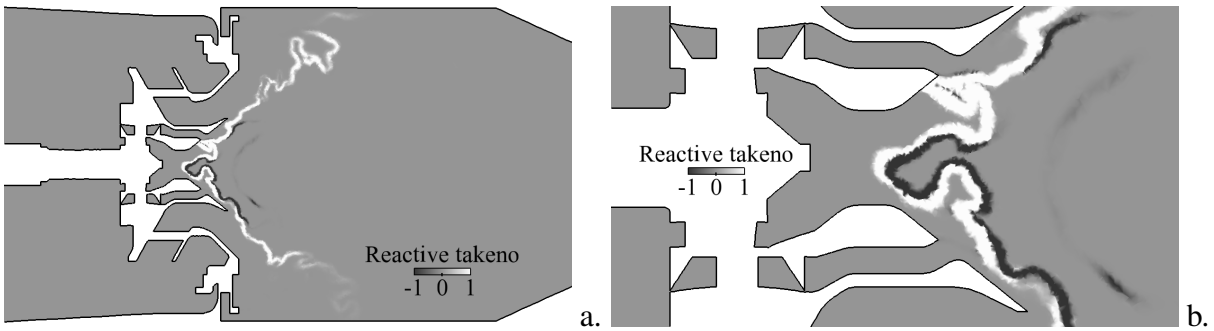

a. b.

Figure 12. (a.) Instantaneous field of normalized Takeno index. (b.) Zoom on the injection region.

to the non-reacting mixing of air at $728K$ with fuel vapor at the wet-bulb temperature $560K$, described by the line $Y_{fuel} = Z$ in Fig. 13a. and the bottom line in Fig. 13b. Note that some points rely below this bottom line as the injected air is slightly cooled by the evaporation process in the unburnt mixture. The second limit corresponds to fully burnt gases, and may be described by an infinitely fast chemistry, diffusion flame solution, *i.e.* two line portions joining at the stoichiometric point (bottom limit in Fig. 13a. and upper limit in Fig. 13b.). Note again that some points lie above the equilibrium temperature: this is another effect of evaporation, this time in the burnt gases, making the fuel vapor concentration increase, *i.e.* moving the burnt gas points towards richer mixture fractions without significantly modifying their temperature. These two limits describe non-premixed situations and the corresponding dots are colored dark by the Takeno index. Between these two limits, a large region is filled with grey dots corresponding to the premixed flame with varying equivalence ratio. A smaller zone just above the non-reacting mixing line is filled with dark points, representing the pre-heating and mixing with burnt gases of the non-homogeneous mixture of air and kerosene vapor just in front of the flame.

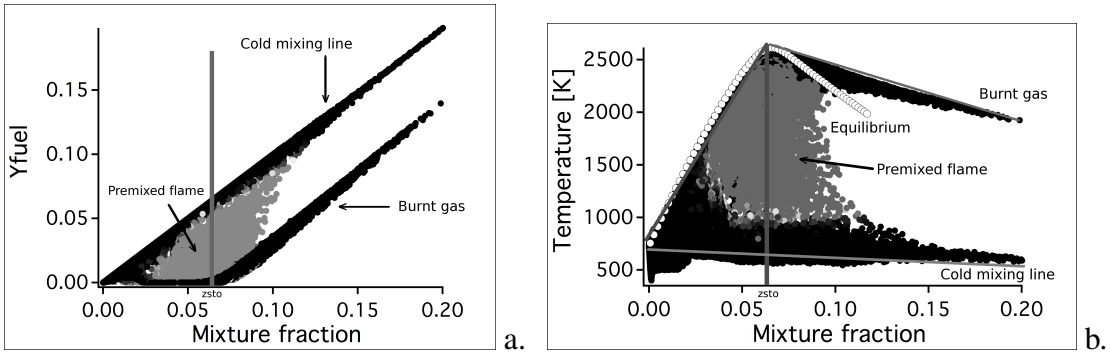

a. b.

Figure 13. Scatter plots of (a.) the fuel vapor mass fraction, and (b.) the gas temperature versus mixture fraction, colored by the Takeno index (grey dots: positive takeno; black dots: negative Takeno index). White symbols represent chemical equilibrium.

The premixed flame burns locally in the mixture fraction range $Z \in [0.03; 0.1]$, *i.e.* $\phi \in [0.5; 1.5]$, higher than the global equivalence ratio of 0.44 and around stoichiometry. The TLC burner allows to strongly stabilize a flame even at a very lean global equivalence ratio. The pilot injector plays a crucial role in this process, as it generates a very energetic flame and a hot gas pocket in the central recirculation zone, which in turn anchors the flame issued from the multipoint injection.

Conclusions

LES was performed in a complex aeronautical burner dedicated to lean spray combustion which presents a complex injection system made of three air swirler stages and two liquid kerosene injections, a pilot injector and a multipoint system. The Euler-Euler approach developed in the AVBP compressible solver was used [5]. The combustion of kerosene was modeled by a two-step reduced scheme and the interaction with turbulence was accounted for using the Thickened Flame model. Injection and evaporation being key phenomena, their modeling was first validated by comparison with experiments in academic configurations. The FIM-UR method [4] was used to reproduce liquid kerosene injection through a pressure swirl atomizer [9]. An improvement of the classical Abramzon-Sirignano evaporation model [17] was proposed to account for the dependence of mixture thermodynamical properties on composition, and then tested in the reference experiment of an evaporating isolated n-heptane droplet [14, 15]. Both models showed good agreements with the experiments and were then used for the two-phase reacting simulation of the TLC burner. Despite its limitations and still many open modeling issues, LES was able to reproduce the crucial role of the pilot injection to stabilise a flame despite the very lean global equivalence ratio. The flame structure analysis showed new behaviours compared to gas flames, mainly due to evaporation: non adiabaticity, change in equivalence ratio across the flame front, diffusion flame far downstream of the premixed flame due to a very rich, oxygen-free burnt gas pocket generated by the pilot spray,... Obviously, some models such as atomization must be improved, and more quantitative comparisons with experiments and LES using an Euler-Lagrange approach are required to improve the analysis of the burner performances. Still, this work raises many questions concerning chemistry modeling (using tabulation methods for instance) or isolated droplet combustion among others.

Acknowledgements

Part of this research project has been supported by the European Community under contract number 210781-2 within the Marie Curie Initial Training Network of the 7^{th} Framework Programme.

References

[1] Ménard, T., Tanguy, S., Berlemont, A., "Coupling level set/VOF/ghost fluid methods: Validation and application to 3D simulation of the primary break-up of a liquid jet", *Int. J. Multiphase Flow* 33:510–524 (2007)

[2] Fuster, D., Bagué, A., Boeckc, T., Moynea, L.L., Leboissetier, A., Popinet, S., Raya, P., Scardovelli, R., Zaleski, S., "Simulation of primary atomization with an octree adaptive mesh refinement and VOF method", *Int. J. Multiphase Flow* 35:550–565 (2009)

[3] Zuzio, D., Estivalezes, J., "An efficient block parallel AMR method for two phase interfacial flow simulations", *Comput. Fluids* 44:339–357 (2011)

[4] Sanjosé, M., Senoner, J., Jaegle, F., Cuenot, B., Moreau, S., Poinsot, T., "Fuel injection model for Euler-Euler and Euler-Lagrange large-eddy simulations of an evaporating spray inside an aeronautical combustor", *Int. J. Multiphase Flow* 37:514–529 (2011)

[5] Boileau, M., Pascaud, S., Riber, E., Cuenot, B., Gicquel, L., Poinsot, T., Cazalens, M., "Investigation of two-fluid methods for Large Eddy Simulation of spray combustion in Gas Turbines", *Flow, Turb. and Combustion* 80(3):291–321 (2008)

[6] Apte, S., Mahesh, K., Moin, P., "Large-eddy simulation of evaporating spray in a coaxial combustor", *Proc. Combust. Inst.* 32(2):2247–2256 (2009)

[7] Jaegle, F., Senoner, J., García, M., Bismes, F., Lecourt, R., Cuenot, B., Poinsot, T., "Eulerian and Lagrangian spray simulations of an aeronautical multipoint injector", *Proc.*

Combust. Inst. 33:2099–2107 (2011)
[8] Lefebvre, A.H., *Atomization and Sprays*, Combustion (Hemisphere Publishing Corporation) (Taylor & Francis, 1989)
[9] Yang, J.T., Chen, A.C., S.H.-Yang, Huang, K.J., "Flow analysis of spray patterns of pressure-swirl micro atomizers", *Pacific Symposium on Flow Visualization and Image Processing* (National Tsing Hua University, 2003), volume 4052
[10] Colin, O., Rudgyard, M., "Development of high-order Taylor-Galerkin schemes for unsteady calculations", *J. Comput. Phys.* 162(2):338–371 (2000)
[11] Ducros, F., Nicoud, F., Poinsot, T., "Wall-adapating local eddy-viscosity models for simulations in complex geometries", *ICFD* (Baines M. J., 1998), pp. 293–300
[12] Poinsot, T., Lele, S., "Boundary conditions for direct simulations of compressible viscous flows", *J. Comput. Phys.* 101(1):104–129 (1992)
[13] Moreau, M., Simonin, O., Bédat, B., "Development of gas-particle Euler-Euler LES approach: A priori analysis of particle sub-grid models in homogeneous isotropic turbulence", *Flow, Turb. and Combustion* 84:295–324 (2010)
[14] Nomura, H., Ujiie, Y., Rath, H.J., Sato, J., Kono, M., "Experimental study on high-pressure droplet evaporation using microgravity conditions", *Proc. Combust. Inst.* 26:1267–1273 (1996)
[15] Chauveau, C., Halter, F., Lalonde, A., Gokalp, I., "An experimental study on the droplet vaporization: effects of heat conduction through the support fiber", *ILASS* (Como Lake, Italy, 2008), 4-1
[16] Sanjosé, M., "Evaluation de la méthode Euler-Euler pour la simulation aux grandes échelles des chambres à carburant liquide", Ph.D. thesis, INP Toulouse (2009)
[17] Abramzon, B., Sirignano, W.A., "Droplet vaporisation model for spray combustion calculations", *Int. J. Heat and Mass Transfer* 9:1605–1618 (1989)
[18] Ranz, W.E., Marshall, W.R., "Evaporation from drops", *Chem. Eng. Prog.* 48(4):173 (1952)
[19] Hubbard, G.L., Denny, V.E., Mills, A.F., "Droplet evaporation: effects of transient and variable properties", *Int. J. Heat and Mass Transfer* 18:1003–1008 (1975)
[20] D.G.Goodwin, *Cantera C++ Users Guide*, http://sourceforge.net/pro jects/cantera (2002)
[21] Bird, R.B., Stewart, W.E., Lighfoot, E.N., *Transport phenomena* (John Wiley, New York, 1960)
[22] Lax, P.D., Wendroff, B., "Difference schemes for hyperbolic equations with high order of accuracy", *Commun. Pure Appl. Math.* 17:381–398 (1964)
[23] Struijs, R., "A multi-dimensional upwind discretization method for the Euler equations on unstructured grids", Phd thesis, Technical University of Delft (1994)
[24] Franzelli, B., Riber, E., Sanjosé, M., Poinsot, T., "A two-step chemical scheme for Large-Eddy Simulation of kerosene-air flames", *Combust. Flame* 157(7):1364–1373 (2010)
[25] Colin, O., Ducros, F., Veynante, D., Poinsot, T., "A thickened flame model for large eddy simulations of turbulent premixed combustion", *Phys. Fluids* 12(7):1843–1863 (2000)